2010 IEEE International Conference on Robotics and Automation
Anchorage Convention District
May 3-8, 2010, Anchorage, Alaska, USA

Path Planning Based on Fluid Mechanics for Mobile Robots Using Unstructured Terrain Models

David Gingras and Érick Dupuis
Space Technologies
Canadian Space Agency
Saint-Hubert, Québec, J3Y 8Y9, Canada
FirstName.LastName@asc-csa.gc.ca

Guy Payre and Jean de Lafontaine
Faculty of Engineering
Université de Sherbrooke
Sherbrooke, Québec, J1K 2R1, Canada
FirstName.LastName@usherbrooke.ca

Abstract— **Mobile robots using a 360° field of view LIDAR ranging sensor can generate enormous 3D point clouds. To reduce the quantity of data in memory a compression can lead to unstructured environment models such as irregular meshes. This kind of structure can contain deformed cells and the path planning can be cumbersome. This paper presents a path planning method based on fluid mechanics able to deal with unstructured terrain models. The algorithm uses the finite element method to compute a velocity potential function free from local minima. Then, several streamlines are computed as a road map and the optimal path is selected among the candidate paths. The approach is implemented on the Canadian Space Agency (CSA) Mars Robotics Testbed (MRT) rover and tested at the CSA Mars Emulation Terrain (MET). To confirm the feasibility of the method, the path planner has been tested on 284 LIDAR scans collected in a realistic outdoor challenging terrain.**

I. INTRODUCTION

Path planning has been a field of research in many areas including mobile robotics, but also in video games, numerical animation, computer aided design (CAD) and even in computational chemistry. In the last few decades, robotics researchers proposed many solutions to generate collision-free paths and trajectories. Generally, these approaches can be classified in three categories : *Road map*, *Cell decomposition* and *Potential field* methods [1]. The current work presents a path planning method that falls into the third category. Indeed, we propose to generate paths from the streamlines of an inviscid fluid flow. This method is mathematically equivalent to the harmonic potential field approach. Presenting the method from a point of view of fluid mechanics is more intuitive because it is based on a physical phenomenon.

Using the finite element method (FEM) in path planning is not new [2]. The major advantage of FEM is the possibility of using it directly on unstructured data such as irregular triangular meshes. That is why this paper also adresses the issue of solving the Laplace equation for the computation of the potential field by FEM. The novelty of the work lies in the application of FEM for path planning on rough terrain models.

The paper first presents the background of the research. Then, a review of the potential flow theory is presented. Next, a method to generate an unstructured terrain model from LIght Detection And Ranging (LIDAR) data is described. Then, the numerical computation strategy follows and the application to path planning is presented in details. Sections VII and VIII describe the results of offline tests and experimental tests conducted on the Canadian Space Agency (CSA) Mars Robotics Testbed (MRT) rover and tested at the CSA Mars Emulation Terrain (MET). Lastly, conclusions are drawn and future directions for the research are proposed.

II. BACKGROUND

The potential field approach invented by Khatib [3] has led the mobile robotics community to a new kind of path planning method based on physical laws. Khatib has proposed an electrostatic analogy where obstacles generate a repulsive field and where the destination is attractive. The article of Koren and Borenstein [4] has explained the well known problem of local minima in the potential field that occurs when the robot runs into a dead-end. Chang has presented a reacting method to escape the trap [5]. On the other hand, Connolly et al. presented a potential field based on Laplace's equation [6]. These authors have discussed that if a potential field is a solution of Laplace's equation, then it is called harmonic function and it has no local minima. After, Connolly presented some useful properties of harmonic functions for robust control [7]. Real time applications of harmonic functions have been presented by Kim and Khosla [8].

The fluid mechanics analogy has been developed first by Keymeulen and Decuyper [9]. They recalled the absence of local minima in the harmonic function and the possible presence of unstable stagnation points. Also, these authors have studied the effect of the Dirichlet and Neumann boundary conditions on the resulting potential field. Louste and Liégeois [10] have explained how to take into account non-holonomic contraints with the viscous fluid field method.

Several of the above-mentioned authors have demontrated several advantages of using the potential field method based on harmonic functions, such as the fluid analogy. This elegant approach can easily generate collision-free paths. Moreover, the resulting paths are continuous, smooth and more intuitive than paths provided by other methods such as graph-based search approaches. However, some authors have presented methods to solve Laplace equation only for a structured terrain model, such as constant resolution cartesian grids [6],

[10] and [11]. Most of them use the *standard finite difference method* to solve the Laplace equation. This approach is built to work only on a structured grid which is not always the best selection for a complex terrain model. This shortcoming was adressed by Pimenta and co-workers [2] with the first application of the FEM to robotics path planning.

The work presented in this paper uses an approach of path plannig based on fluid mechanics, which is able to take as input unstructured and uneven terrain models based on irregular meshes. The motivation for using an irregular mesh came from the compression of the enormous amount of data provided by a 360° LIDAR scan. To store in memory all the rover surrounding data, it is sufficient to generate a mesh from LIDAR data and simplify it via a mesh simplification algorithm, which reduces the number of cells while preserving the shape and topography [12], [13] and [14]. The resulting mesh is compact but unstructured because it contains cells of different sizes and geometry. The standard finite difference method cannot be used on this kind of terrain model. That is why FEM is adopted here to solve the Laplace equation. Differently from Pimenta et al., who also used FEM, the present work generates a feasible *road map* and selects an optimal path. Moreover, another improvement with respect to previous works is the application of FEM to rough and uneven terrain models.

III. POTENTIAL FLOW THEORY

Let us outline the mathematical model describing the flow of an inviscid incompressible fluid. Assuming a steady irrotational flow in the Eulerian framework, the velocity field V obeys the relation

$$\nabla \times V = 0. \tag{1}$$

As a consequence, velocity is the gradient of a scalar (potential) function ϕ, $V = -\nabla\phi$. Conservation of mass for a steady incompressible flow results in the expression $\nabla \cdot V = 0$, so that the potential ϕ is harmonic (solution of the Laplace equation)

$$\nabla^2\phi = 0, \tag{2}$$

inside any volume where conservation of mass holds. A localized fluid source (or a sink) can be modeled by a Dirac term (δ) added to the right hand side of (2). Assuming a unit amount of fluid injected at point A during a unit of time and the same unit withdrawn at point B, the velocity potential is now solution of the Poisson equation:

$$-\nabla^2\phi = \delta_A - \delta_B. \tag{3}$$

Equation (3) must be complemented by appropriate boundary conditions. The fluid cannot flow through the boundaries, a condition expressed by $V \cdot n = 0$ (n being a vector normal to the boundary Γ). On Γ the velocity potential must verify:

$$\nabla\phi \cdot n = 0, \tag{4}$$

which amounts to the Neumann boundary conditions:

$$\left.\frac{\partial\phi}{\partial n}\right|_{\Gamma} = 0. \tag{5}$$

Resolution of the Poisson equation can be achieved by several approaches. Section V explains how to obtain the potential ϕ of (3) on an *irregular triangular mesh* (ITM). The next step is the computation of the velocity field. As explained before, the velocity of the flow can be computed everywhere on the domain by the gradient of the potential. For path planning purposes, the magnitude of velocity vectors is not useful (only the direction is needed) and the vector field V can be normalized.

IV. UNSTRUCTURED TERRAIN MODEL

This Section presents a strategy to get a terrain model from a raw point cloud provided by a 360° LIDAR sensor [14]. The model is an input of the path planning algorithm. The complexity of the model must remain low in order to limit the path planning computational time. The complexity of the model is a tradeoff betwen computational time and accuracy.

A. Mesh building and processing

When raw LIDAR data are acquired, an ITM is built from the 3D point cloud. The approach is explained in details in [14]. The triangular mesh is obtained using the *Delaunay triangulation* [15] applied on the point cloud expressed in polar coordinates. The resulting mesh can contain thousands of triangles depending on the resolution of the raw scan. Then, in order to reduce the quantity of redundant information, the mesh is compressed via a simplification method using *QSlim* algorithm [16].

To keep only the navigable region of the ITM, a filter removes the triangles whose slope is too steep. This step leads to a mesh without "walls" and "ceilling" and where only the terrain without rocks and inclines is preserved. Then a Laplacian smoothing filter is applied to improve the mesh quality. Figure 1 shows an example of an ITM built from a real LIDAR scan taken by the CSA MRT at the MET.

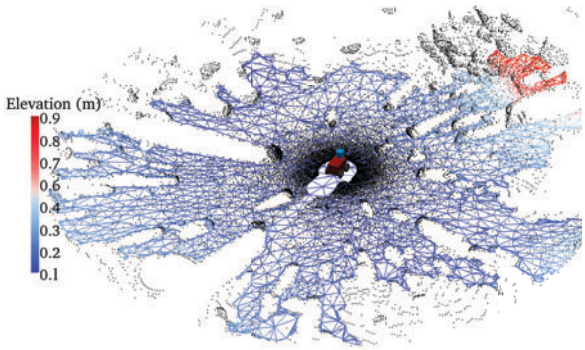

Fig. 1. ITM and the corresponding LIDAR scan (black point cloud)

In Fig. 1 a rover is also drawn to show the context of the measurement. The point cloud contains 110,000 3D points. The colored surface is the resulting mesh that contains 3,960 triangles. The maximum radius of the LIDAR scan is 10 m.

V. NUMERICAL COMPUTATION

This Section deals with the numerical approximation of the velocity field on a triangular mesh . One has first to compute the potential ϕ, solution of the Poisson equation, deducing next the velocity field V.

A. Approximation of the potential

For decades, the finite element method has been widely used for the computation of potential functions. This paper does not provide details of the method (the reader can refer to [17] for further details). The FEM splits the domain into a finite set of cells, assuming a given (usually polynomial) shape of the state function inside each cell. This discretization reduces the problem to the computation of a finite number of unknowns, which is performed by solving a linear system. In our case, we can make direct use of the unstructured mesh data obtained in the previous step as input to a finite element solver. Using a linear *Lagrange interpolation* inside each triangle e with vertices (i,j,k), the approximated potential takes the form:

$$\phi^e(x,y) = \phi_i N_i^e(x,y) + \phi_j N_j^e(x,y) + \phi_k N_k^e(x,y), \qquad (6)$$

where the shape function N_i^e is linear inside each cell, N_i^e takes the value 1 on vertex i and is equal to 0 for all other mesh vertices. Fig. 2 presents an example of FEM problem for a first order triangular mesh.

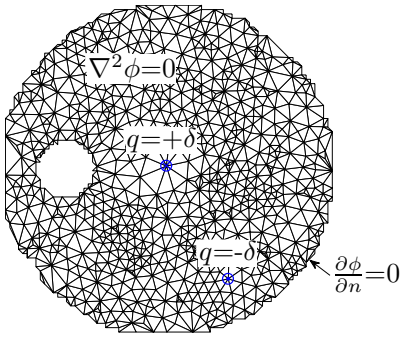

Fig. 2. Example of FEM problem with one source and one sink on a simple mesh

Figure 2 outlines the problem of potential flow according to (3). There are a source with a positive volumetric flow (represented by $\otimes$ with $q=+\delta$) and a sink (indicated by $\odot$ with $q=-\delta$). Elsewhere, the Laplacian of the potential is zero ($q=0$). Moreover, homogeneous Neumann boundary conditions are applied as required by (5). Figure 3 shows the velocity potential ϕ of the example of Fig. 2 as computed by FEM.

As shown in Fig. 3, there is no local extremum in any region excluding the source and the sink. The source is at a global maximum of the function and the sink at a global minimum.

B. Computation of the velocity field

As proposed by the fluid flow analogy, the vector field needed to guide the robot from an initial position to its destination is identified with the fluid velocity, gradient of the potential. To compute this direction inside a triangle, one has simply to take the gradient of (6), that is:

$$V^e = -\nabla\phi^e(x,y) = -\phi_i \nabla N_i^e - \phi_j \nabla N_j^e - \phi_k \nabla N_k^e. \qquad (7)$$

Figure 4 shows the velocity field of the example of Fig. 2. As expected, velocity vectors are nearly perpendicular to potential isovalues. This vector field is used to generate paths from the initial position to the destination.

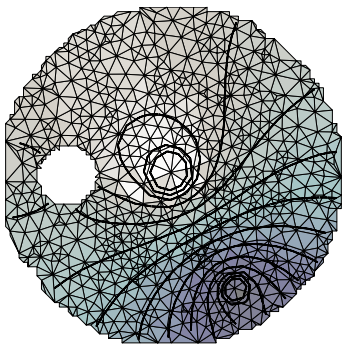

Fig. 3. Velocity potential (black isovalue lines) solved by FEM for the example of Fig. 2

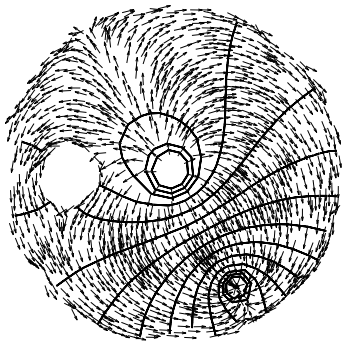

Fig. 4. Velocity field for the example of Fig. 2

VI. PATH PLANNING

This Section describes how to extract a safe and optimal path between an initial position and a destination from the velocity field and the terrain model. The idea to generate a path is to plot a streamline by following a fluid molecule flowing from the source towards the sink. Following several molecules leads to several streamlines and a *road map* can be built. Then, an optimal path can be selected inside the candidate paths available within the *road map*.

A. Streamline computation

In fluid mechanics, a *streamline* is the path followed by a fluid molecule along its spatial displacement. For the steady state case, streamlines are tangent to the velocity vectors. Then, a streamline can be drawn by starting near the source at an arbitrary location, following the velocity vector until the vicinity of the sink. A number of streamlines can be plotted by starting in several locations surrounding the source. Figure

5 shows some of the streamlines computed from the velocity field of Fig. 4.

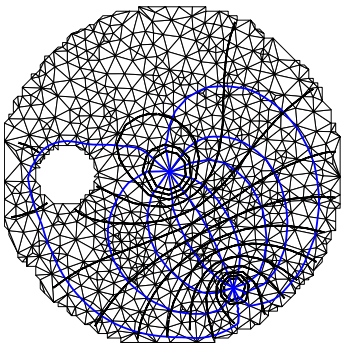

Fig. 5. Streamlines (blue lines) of the flow for the example of Fig. 2

B. Road map building

In robotics, the concept of *road map* can be described as a set of candidate paths between an initial position and a destination. A *road map* can be built by projecting all the 2D streamlines on the 3D terrain model. To this end, the elevation of each point of the streamlines is computed using the Lagrange interpolation method as shown in Subsection V-B. When all streamlines are converted into 3D lines, an analysis of the feasibility of each of the 3D candidate paths is performed. The feasibility of each waypoint of a path is tested. If a waypoint reaches an obstacle, the whole path associated to that point is rejected. When alls waypoints of each path are verified, only safe paths are selected for the *road map*. The path planner proposed in this paper deals with three kinds of obstacle:

1) slope too high;
2) roughness too high (e.g. rocks, abrupt craters);
3) unknown area (not sensed by the LIDAR).

To detect these obstacles at a waypoint position, a discrete rover footprint is used. Figure 6 illustrates an example of a rover seen from the top along with its circular footprint.

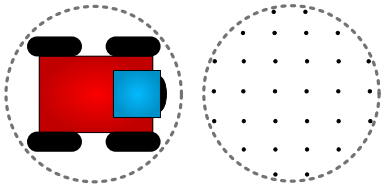

Fig. 6. Robot and circular discret footprint

To test the feasibility of a waypoint, the footprint is centered at the position of the waypoint and each discrete point is projected on the ground. Lagrange interpolation is used again to compute the elevation of every footprint points. To apply the interpolation, first the triangle supporting the discrete point has to be found. If there is no triangle associated to a footprint point, it means that a part of the footprint is outside the terrain model. So this tested position can be declared unsafe according to obstacle definition 3) if the rover is not considered like a point-robot.

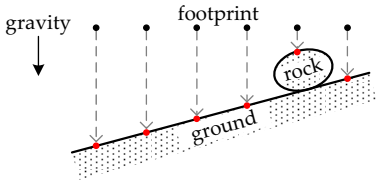

(a) Projection of the footprint on the ground

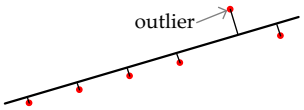

(b) Computation of a least square plane

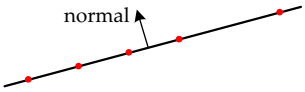

(c) Rejection of outliers and computation of the second least square plane

Fig. 7. Computation of a terrain slope with "intelligent" surface mean plane approach

When the whole 3D footprint is obtained, the local average slope can be computed. The *"Intelligent" surface mean plane* approach discussed in [18] leads to a computation of a local slope without the disturbance stemming from high roughness. Basically, the method computes first a mean plane passing through the point cloud using least square method. Then, the point/plane distance is computed for each point. High roughness obstacles like rocks are detected by a statistical analysis of the point/plane distance. Points outside a few standard deviations are rejected. Finally, a second plane is computed without the influence of high roughness. Figure 7 gives an example of the approach used to compute an approximation of the local slope.

The local slope of the ground is given by the angle between the gravity vector and the surface normal vector. The local roughness can be analysed also with the point/plane distance. The distance between each point of the 3D footprint and the "intelligent" surface mean plane is computed. The maximum point/plane distance is the highest roughness located in the radius of the footprint.

As a final result, the *road map* contains only safe paths with waypoints where the local average slope and the highest roughness are below the thresholds imposed by the rover's operational limits. The last step is the selection of the optimal path among the candidate paths of the *road map*.

C. Optimal path selection

The *road map* contains a list of safe paths. The number of candidate paths depends on the number of streamlines generated (based on the 2009 field test campaign, this number is 20). The selection of the optimal path available can be based on several criteria (length, energy, curvature, etc.). This project uses only the following criteria for paths analysis:

1) total length, and
2) energy consumption.

For each path of the *road map*, both criteria are computed and two numbers can be associated to each path. One is associated to the total length and the other is proportionnal to the energy consumed to follow the path. The 3D length l is simply computed as the sum of segments composing a path:

$$l = \sum_{i=2}^{n} \|P_i - P_{i-1}\|, \tag{8}$$

where P_i is the 3D position vector of the waypoint i, and n is the number of waypoints for a path. For the analysis of energy consumption, only the gravitational potential associated to change in elevation is considered. So for every paths, the elevation gain l_{z+} is computed by:

$$l_{z+} = \sum_{i=2}^{n} \alpha_i, \tag{9}$$

where α_i is defined as follows:

$$\alpha_i = \begin{cases} P_{i_z} - P_{i-1_z}, & P_{i_z} - P_{i-1_z} > 0 \quad (10a) \\ 0, & \text{otherwise.} \quad (10b) \end{cases}$$

The term P_{i_z} is the elevation of waypoint i. When all paths of the *road map* are analysed with each criterion defined by (8) and (9), a cost can be associated to each path. The values of length and energy are normalized and indicated by $\hat{l}$ and $\hat{l}_{z+}$. The cost C can be computed for each path with the following expression:

$$C = \beta_l \hat{l} + \beta_{l_{z+}} \hat{l}_{z+}\ , \tag{11}$$

where β_l et $\beta_{l_{z+}}$ are weighting positive values. Finally, the selected path is the one with the lowest cost.

VII. REAL WORLD IMPLEMENTATION

This Section describes an implementation of the above described path planner on the Canadian Space Agency Mars Rover Testbed (MRT). The MRT is operated in an outdoor laboratory (MET) of 60 m by 30 m that emulates the topography of a martian terrain. MET features several rocks of different dimensions, craters along with a mountain, a plain, a cave and a cliff. The MRT is a modified Pioneer P2AT mobile robot manifactured by ActivMedia. The rover is equipped with a SICK LIDAR mounted on a rotating pan unit leading to a 360° field of view vision sensor. The robot has onboard a Panasonic Toughbook laptop with Intel Core 2 processor running Linux operating system. Figure 8 (a) shows the CSA testbed. The high level autonomy algorithms are coded in JAVA and implemented in Eclipse 3.5. The path planner and the terrain modeler are coded in Matlab scripts and deployed to JAVA with the Builder-JA Toolbox of Mathworks. The finite element solver is coded in *C-mex* script.

Figure 8 presents the data collected in the field. The black point clouds shown in Fig. 8 (b) and Fig. 8 (c) are the raw LIDAR data, the colored surface is the processed mesh used by the path planner and the blue line is the path computed. Figure 8 (a) is a photo of the experimental set-up. Figure 8 (a) shows the tracks left by the rover on the ground. This pattern follows the path generated by the planner algorithm. The experiment[1] presented at Fig. 8 used the rover parameters shown at Table I. For the optimal path selection, the path planner used a length weight β_l of 2.5 and energy weigth $\beta_{l_{z+}}$ of 1.0. Also, the planner has generated 20 streamlines for the contruction of the road map.

(a) Experimental set-up

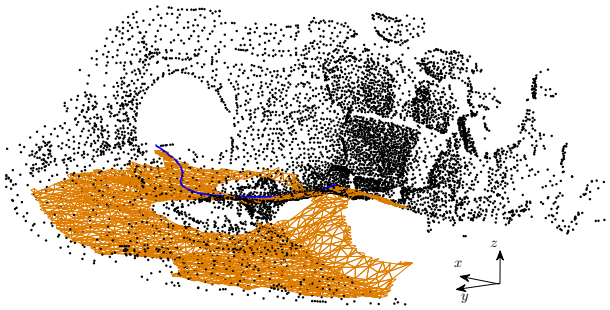

(b) Data collected in the field

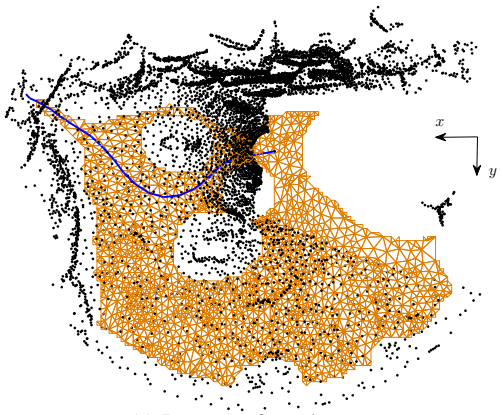

(c) Data seen from the top

Fig. 8. Path generated online by the rover move into a cave

Other experimental results are shown at Fig. 9, where the colored surface represents the assembly of every meshes

[1]A video presenting this experiment is available online: http://www.gel.usherbrooke.ca/icra2010/davidgingras

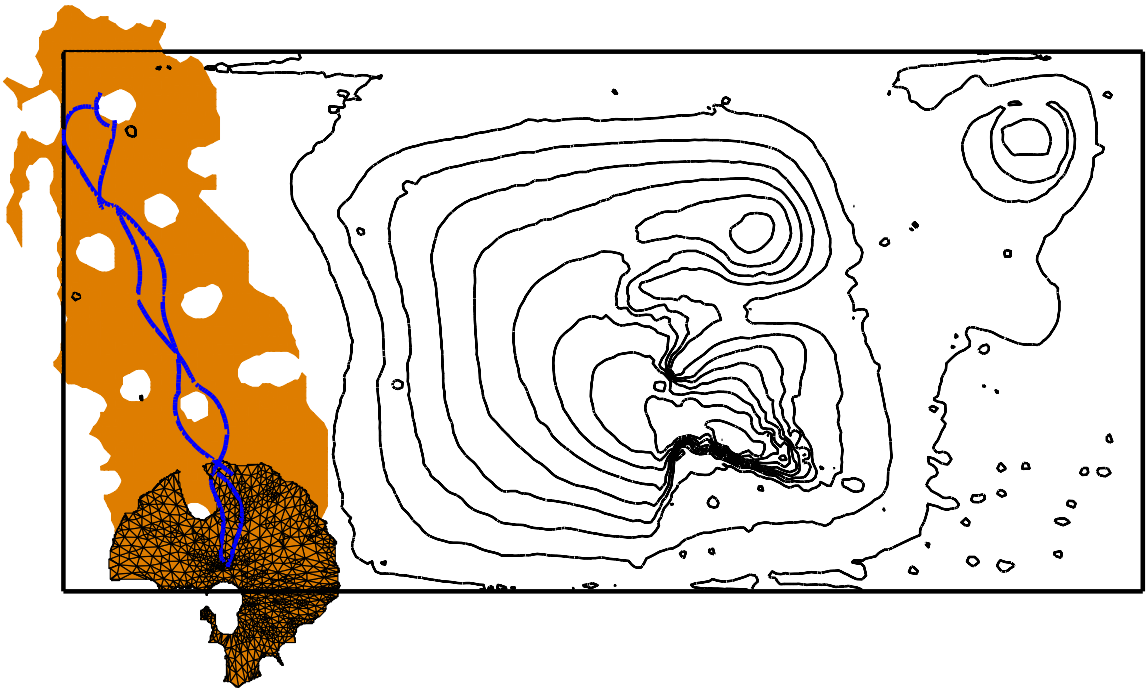

Fig. 9. Closed path performed on MET

TABLE I
ROVER PARAMETERS USED BY PATH PLANNER

Rover radius	Footprint res.	Slope limit	Roughness limit
35.0 cm	2.0 cm	25.0°	10.0 cm

collected on the way to destination. Only edges of the first mesh are shown. The black lines are the isocontours of the digital elevation map of MET. Paths are represented by blue lines. The start configuration of the rover is at the bottom of Fig. 9. The first requested destination is at the top left. The robot took LIDAR scans, meshed the data, generated paths and localised itself autonomously. The details of the whole autonomy approach are explained in [19]. To make a closed path, a second destination was sent to the rover to bring it back to the initial position. Each local path generated by the rover (there are 11 paths in Fig. 9) was computed with the fluid mechanics approach described here. The rover has autonomously traveled 63.9 m.

VIII. OFFLINE VALIDATION

To validate the functionality of the algorithm and to characterize its performance, the path planner is tested offline with a database of 284 LIDAR scans. Those scans have been collected using the CSA MRT during the test campaigns of 2007, 2008 and 2009. During these campaigns, the autonomy algorithms were tested and all experiment data were stored including the LIDAR scans. A batch processing job executed the following steps to test the path planner with every scans:

1) load a raw LIDAR scan;
2) generate a triangular mesh;
3) generate a random destination close to the mesh boundary;
4) confirm the feasibility of the destination and find another destination if it is needed;
5) run the path planner;
6) save the results;
7) restart from 1) until each scan is processed.

This offline experiment saves as results the values of:

- the number of points inside the LIDAR scan;
- the number of mesh triangles;
- the meshing computation time; and
- the path planning computation time.

A snapshot of the resulting scene is also generated in order to allow a visual inspection of each generated path. The offline tests were conducted with a Laptop Dell Latitude equipped with a Intel Core 2 processor, 2.0 GB of RAM memory and a Linux operating system. The numerical parameters used are the same as Table I. To study the behavior of the path-planning algorithm over different mesh accuracies, the batch job is run thrice with a different number of mesh triangles. For those experiments, the targeted number of mesh triangles is 1,500, 4,000 and 8,000. The robot is assumed to be centered in the middle of a 7 m radius mesh. The Table II and III present the results.

The mesh processing time is almost the same for each test. The path planning computation time shown in Table III is associated to the number of mesh triangles. In fact, the finite element solver embedded in the path planner has an algorithm complexity of $O(n^3)$ where n is the number of mesh vertices and there exists a link between the number of mesh vertices and the number of mesh triangles. This

TABLE II

MESH AVERAGE RESULTING VALUES OF THE BATCH PROCESSING TESTS

Exp.	LIDAR scan nb. of pts.	Triangle nb.	Comp. time (s)
1	96,400	1,455	19.4
2	96,400	3,957	19.2
3	96,400	7,938	19.8

TABLE III

PATH PLANNER RESULTS OF THE BATCH PROCESSING TESTS

Exp.	Average comp. time (s)	Standard dev. (s)	Faillure (%)
1	2.3	1.1	2.5
2	5.7	1.8	2.1
3	14.7	3.4	1.4

explains why the path-planning processing time grows with the number of mesh triangles. Visual inspection of the failure cases has revealed that the failures of the path planner were due to the impossibility of safely driving the rover from start to destination. Failure causes included disconnected cells or untraversable terrain.

IX. CONCLUSIONS AND FUTURE WORKS

The purpose of this research project was to develop a path planning approach that uses as input an unstructured mesh that models an uneven terrain. Because of the possible presence of deformed cells in this type of model, the artificial potential field method is preferred to graph search. Path planning based on graph search applied to an unstructured mesh leads often to very jagged paths. To avoid the well-known local minima problem of the potential field method, we used a fluid mechanics analogy building an harmonic potential field free of local minima. This kind of approach relies on the solution of Laplace's equation. The FEM was used because of the irregular mesh.

To demonstrate the feasibility and to assess the performance of our approach, the algorithms have been tested on 284 LIDAR scans collected on an outdoor challenging terrain. The path planner is currently deployed and used by Canadian Space Agency on the Mars Robotics Testbed. The CSA rover using the above outlined path planner was operated from the International Space Station during the Avatar Explore Space Mission that took place in 2009. For more information about the Avatar project, the reader can refer to the paper of Dupuis et al. [20].

Finally, we are currently developing a hybrid path planner based on graph search and fluid mechanics to take advantage of both methods. A graph search path planner can provide a good first estimate of a path to follow and the fluid method can refine and increase the quality of the resulting path.

ACKNOWLEDGMENTS

The authors acknowledge each developers of the Canadian Space Agency Mobile Robotics Testbed. Thanks are also extended to Dr. Alessio Salerno and Jean-Luc Bedwani both engineers at CSA. They provided useful help during the development, in the field and in reviewing of the paper. The work described in this article was carried out under the Space Technologies Research Program at CSA.

REFERENCES

[1] J.-C. Latombe, *Robot motion planning*. Kluwer Academic Publishers, Boston, MA, 1991.

[2] L.C.A. Pimenta, A.R. Fonseca, G.A.S. Pereira, R.C. Mesquita, E.J. Silva, W.M. Caminhas, and M.F.M. Campos, "On Computing Complex Navigation Functions," in *IEEE International Conference on Robotics and Automation (ICRA)*, Barcelona, Spain, Apr. 2005, pp. 3452–3457.

[3] O. Khatib, "Real-Time Obstacle Avoidance for Manipulators and Mobile Robots," *The International Journal of Robotics Research*, vol. 5, no. 1, pp. 90–98, 1986.

[4] Y. Koren and J. Borenstein, "Potential Field Methods and their Inherent Limitations for Mobile Robot Navigation," in *IEEE International Conference on Robotics and Automation (ICRA)*, vol. 2, Sacremento, CA, Apr. 1991, pp. 1398–1404.

[5] H. Chang, "A New Technique to Handle Local Minimum for Imperfect Potential Field Based Motion Planning," in *IEEE International Conference on Robotics and Automation (ICRA)*, vol. 1, Minneapolis, MN, Apr. 1996, pp. 108–112.

[6] C.I. Connolly , J.B. Burns, and R. Weiss, "Path Planning Using Laplace's Equation," in *IEEE International Conference on Robotics and Automation (ICRA)*, vol. 3, Cincinnati, OH, May 1990, pp. 2102–2106.

[7] C.I. Connolly, "Applications of Harmonic Functions to Robotics," in *IEEE International Symposium on Intelligent Control*, Glasgow, UK, Aug. 1992, pp. 498–502.

[8] J.-O. Kim and P.K. Khosla, "Real-time Obstacle Avoidance Using Harmonic Potential Functions," *IEEE Transactions on Robotics and Automation*, vol. 8, no. 3, pp. 338–349, June 1992.

[9] D. Keymeulen and J. Decuyper, "The Fluid Dynamics Applied to Mobile Robot Motion: The Stream Field Method," in *IEEE International Conference on Robotics and Automation (ICRA)*, vol. 1, San Diego, CA, May 1994, pp. 378–385.

[10] C. Louste and A. Liégeois, "Path Planning for Non-Holonomic Vehicles: A Potential Viscous Fluid Field Method," *Robotica*, vol. 20, no. 3, pp. 291–298, 2002.

[11] Z.X. Li and T.D. Bui, "Robot path planning using fluid model," *Journal of Intelligent and Robotic Systems*, vol. 21, no. 1, pp. 29–50, 1998.

[12] E. Dupuis, I. Rekleitis, J.-L. Bedwani, D. Gingras, P. Allard, T. Lamarche, and W.H. Zhu, "Autonomous Over-The-Horizon Rover Navigation," in *10th ESA Workshop on Advanced Space Technologies for Robotics and Automation (ASTRA)*, Noordwijk, The Netherlands, Nov. 2008.

[13] I. Rekleitis, J.-L. Bedwani, D. Gingras, and E. Dupuis, "Experimental Results for Over-the-Horizon Planetary Exploration Using a LIDAR Sensor," in *11th International Symposium on Experimental Robotics (ISER)*, vol. 54, Athens, Greece, Mar. 2009, pp. 65–77.

[14] D. Gingras, T. Lamarche, J.-L. Bebwani, and E. Dupuis, "Rough Terrain Reconstruction for Rover Motion Planning," *submited to the 7th Canadian Conference on Computer and Robot Vision (CRV)*, 2010.

[15] B. Delaunay, "Sur la Sphere Vide : Bulletin of the Academy of Sciences of the USSR," *Classe des Sciences Mathematiques et Naturelles*, vol. 8, pp. 793–800, 1934.

[16] M. Garland and P.S. Heckbert, "Surface Simplification Using Quadric Error Metrics," in *Proceedings of the 24th annual international conference on Computer graphics and interactive techniques (SIGGRAPH)*, Los Angeles, CA, Aug. 1997, pp. 209–216.

[17] O.C. Zienkiewicz, *The Finite Element Method*, 3rd ed. London: McGraw-Hill, 1977.

[18] J. de Lafontaine and O. Gueye, "Autonomous planetary landing using a lidar sensor: The navigation function," *Space Technology*, vol. 24, 2004.

[19] E. Dupuis, I. Rekleitis, J.-L. Bedwani, T. Lamarche, P. Allard, and W.H. Zhu, "Over-The-Horizon Autonomous Rover Navigation: Experimental Results," in *Proceedings of the 9th International Symposium on Artificial Intelligence, Robotics and Automation in Space (iSAIRAS)*, Los Angeles, CA, 2008.

[20] E. Dupuis, P. Langlois, J.-L. Bedwani, D. Gingras, A. Salerno, P. Allard, S. Gemme, R. L'Archevêque, and T. Lamarche, "The Avatar Explore Experiments: Results and Lessons Learned," in *abstract submitted to International Symposium on Artificial Intelligence, Robotics and Automation in Space (iSAIRAS)*, Hokkaido, Japan, January 2010.